Differential Molecular Interactions of Telmisartan: Molecular-Level Insights from Spectral and Computational Studies

Mahendra Singh[1], Jacob Kongsted[2], Peng Zhan[3], Uttam Chand Banerjee[1], Vasanthanathan Poongavanam[2], and N. Arul Murugan[4]*

[1]Department of Pharmaceutical Technology (Formulations), National Institute of Pharmaceutical Education and Research (NIPER), Sector 67, S.A.S. Nagar (Mohali), India.

[2] Department of Physics, Chemistry, and Pharmacy, University of Southern Denmark, DK-5230 Odense M, Denmark.

[3] Key laboratory of Chemical Biology (Ministry of Education), School of Pharmaceutical Sciences, Shandong University, 44 Wenhua xi Road, Jinan, 250012, P.R. China.

[4] Department of Theoretical Chemistry and Biology, School of Engineering Sciences in Chemistry, Biotechnology and Health, Royal Institute of Technology, Stockholm, Sweden.

Corresponding Author

N. Arul Murugan

Department of Computer Science, School of Electrical Engineering and Computer Science, KTH Royal Institute of Technology, Stockholm, Sweden.

E-mail: arul.murugan.at.kth@gmail.com

Abstract

In this study, we investigated differential molecular interactions of crystalline and amorphous forms of telmisartan (TEL), which is a non-peptide angiotensin-II receptor antagonist commonly used in the management of hypertension. Amorphous telmisartan (AM-TEL) was prepared using quench cooling of the melt. The analysis of solid-state properties of AM-TEL using differential scanning calorimetry (DSC) and X-ray powder diffraction (XRD) confirmed formation of AM-TEL. Based on a comparative analysis of molecular interactions using spectral (FTIR and ^{13}C solid-state NMR) and computational tools, we demonstrated that amorphous telmisartan shows altered molecular interactions. Molecular dynamics simulation of amorphous and crystalline forms demonstrate that the amorphous form retained some of molecular interactions in its disordered molecular arrangement, with a relatively stronger (decrease in bond length) but lesser (up to only 2.6 % of the population) hydrogen bonding network as compared with the crystalline counterpart (up to 76% of the population).

Keywords: Telmisartan, Differential molecular interactions, Hydrogen bonding, Spectroscopy, Simulated annealing, Molecular dynamics.

1 Introduction

New drug discovery approaches such as high-throughput screening [1] and computer-aided drug design [2] have changed the paradigm of drug discovery and generated libraries of potential drug molecules. However, statistically, 70% of these new drug molecules are highly lipophilic with high molecular weight and eventually fail to enter the product development phase primarily due to their sub-optimum aqueous solubility [3] which is one of the essential physicochemical parameters that direct the bioavailability of drug molecules [4]. Hence, in the early drug development phase, alternative solid-state forms like different polymorphs [5,6], salts [7,8], co-crystals [9] and amorphous solids [10] are screened for achieving adequate aqueous solubility. For instance, solubility of indomethacin [11], celecoxib [12], indapamide [13] and atorvastatin calcium [14] has been significantly improved with their amorphous solid forms. This aqueous solubility advantages led amorphous solids to show higher bioavailability in comparison to their crystalline counterparts. Structurally, amorphous solids lack three-dimensional long-range order symmetry operators (conformational, orientational, and translational), characteristics of the crystalline solids [15]. Thermodynamically, amorphous solids differ from the crystalline solids by having higher Gibbs free energy, volume, entropy, enthalpy and a characteristic glass transition temperature [16] . All these differences mentioned above together are bound for the higher

apparent solubility, molecular mobility, intrinsic dissolution rate, surface activity, chemical reactivity and processability of amorphous solids [17]. However, despite a number of advantages of amorphous solids over their crystalline counterparts, amorphous solids are far from the widespread use and there are only very few products in the market containing neat amorphous API, for instance, Accolate®, Ceftin®, Accupril® and Viracept® [18–20]. Typically, the major cause after the paucity of neat amorphous API-based formulations in the commercial market is their thermodynamic instability and unpredictability of crystallization potential during processing and storage [21]. Furthermore, the insufficiency of a fundamental and thorough molecular-level understanding of amorphous solids is also another reason. A plenty of literature has been published on amorphous pharmaceutical solids [22]. However, there are very few explanations on the molecular level information of amorphous solids [23,24]. Hence, a thorough and comparative investigation into the molecular interactions in amorphous solids and their differences from their crystalline counterparts might help in designing novel amorphous phase-based formulations. Telmisartan (TEL, Fig. 1) is one of the most prescribed orally active non-peptide angiotensin II receptor antagonist used to treat essential hypertension [25]. TEL is a highly permeable molecule (log P 6.04) [26] with extremely pH dependent [27] low aqueous solubility (0.09 μg/mL). The parameters mentioned above classify TEL as a BCS class II drug [28]. Furthermore, determination of dimensionless biopharmaceutical parameters like dose number and dissolution number [29] revealed the dissolution rate limited oral bioavailability (40-58%) of TEL [30]. Consequently, in the quest for higher dissolution rate, different strategies, including alternative solid-state forms like polymorphs [31], salts, cocrystals [32] and amorphous form of TEL [33] have been generated and investigated.

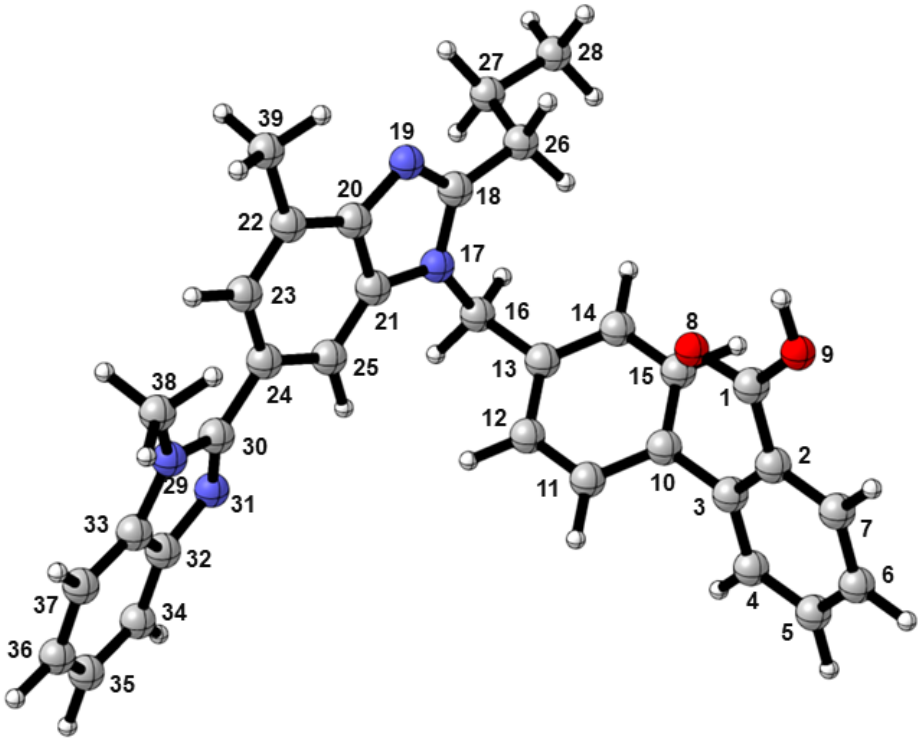

MW (g.mol^{-1})	log P	HBA	HBD	PSA (Å^2)	NRotB
514.63	6.04	4	1	72.94	7

Fig. 1. Chemical structure of telmisartan and its physicochemical properties

Dinnebier et al. [31] reported three crystalline polymorphs (Form A, B and C) of TEL and showed that close intermolecular contacts of methyl and n-propyl substituents of benzimidazole rings, parallel stacking of central benzimidazole rings, π-π interaction and a hydrogen bond are the major characteristic features in structural organization of polymorph A. The very few research groups have prepared and investigated amorphous telmisartan (AM-TEL). Adrjanowicz et al. [34] prepared AM-TEL using cryo-milling and quench cooling method and comprehensively investigated stability (physical and chemical), molecular mobility and solubility advantage over crystalline telmisartan (CR-TEL) counterpart. Furthermore, Moura et al. [33] revealed the high glass-forming ability and the moderate glass stability of AM-TEL. However, all these studies leave a gap in studying the differences in molecular interactions of AM-TEL and CR-TEL. In current study, AM-TEL was prepared by quench cooling of melt and differences in the molecular interactions were investigated using the spectral (FTIR and solid-state ^{13}C NMR studies) and computational tools. CR-TEL and AM-TEL were studied by force-field-based molecular dynamics approach and various structural and energetic properties were analyzed.

This is, to our knowledge, the first time that the information from different methods has been used to investigate the microstructure of AM-TEL and CR-TEL in detail.

2 Materials and methods

2.1 Materials

CR-TEL (Polymorph A) was purchased from All Well Pharmaceuticals Co. Limited (Chandigarh, India) and received as a white crystalline powder (> 95 % purity). The purity of CR-TEL was checked with high-performance liquid chromatography (Supporting information, Fig. S1).

2.2 Methods

2.2.1 Preparation of AM-TEL.

AM-TEL was prepared by previously reported quench cooling of the melt method [34]. Briefly, CR-TEL was placed in a steel bowl, and then steel bowl was put into the muffle furnace (laboratory model NSW-101, Narang scientific works Pvt. Ltd.) maintained at 274°C (5°C more than the melting point of CR-TEL). After complete melting (holding for 1 min to ensure complete melting), sample was quench cooled in an ice-cold beaker. The color, temperature, and exposure of AM-TEL to water vapor were carefully checked and no visible sign of degradation was observed. Subsequently, AM-TEL was analyzed immediately after its preparation.

2.2.2 Fourier-transform infrared (FTIR) spectroscopy.

FTIR spectrophotometer (Spectrum One, Perkin-Elmer, Buckinghamshire, U.K.) was used to record the FTIR spectra of CR-TEL and AM-TEL. Attenuated total reflection (ATR) technique was employed and the background spectrum was collected under identical conditions. Each spectrum was derived from 10 single averaged scans collected in the region 650-4000 cm^{-1} at a spectral resolution of 4 cm^{-1}. The recorded spectra were analyzed using the Spectrum software (version v 5.0.1).

2.2.3 Computational studies.

The Mercury software (version 4.0.0, CCDC, Cambridge, UK) [35] was used to construct a unit cell of TEL from single crystal X-ray diffractometry data and the hydrogen bonding pattern in CR-TEL was analysed. This information was used to interpret any shifts in the FTIR peaks in AM-TEL. In addition to this, finite temperature structures for CR-TEL and AM-TEL were

studied using a force-field-based molecular dynamics approach. Initially, 6x6x6 unit cells of TEL were prepared using the Mercury software. This has been used as an input structure for studying the crystal structure and for exploring the amorphous form of the compound. The crystal form is heated until it becomes liquid and then quenched to a low temperature to become amorphous. The formed amorphous phase retained its structure during the entire simulation. The phase transition temperatures for molecular crystals can be different in simulations when compared to experimental values. This difference in transition temperatures has been attributed to the superheating effect and system size in computational models. Both CR-TEL and AM-TEL were studied at 200 K and 1 atmospheric pressure. The calculations were carried out in the isothermal-isobaric ensemble using the Amber software (version 21)[36]. The force-field for TEL was based on the GAFF (general amber force-field). The partial atomic charges were obtained by fitting to the molecular electrostatic potential and by using the CHELPG method as implemented in Gaussian 09 [37]. In particular, we employed the B3LYP/6-31+G* level of theory for computing the charges. The time step for the integration of equation of motion was set to 1 fs, the equilibration run was carried out for 2 ns and the timescale for the production run was 10 ns. Various structural and energetic properties were analyzed for the convergence which suggests the simulation length scale was sufficient**.** Hydrogen bond analysis for CR-TEL and AM-TEL was carried out using cpptraj module [38] available in amber tools. The analysis also involved estimating the population of intramolecular and intermolecular hydrogen bonds and their average geometrical values.

2.2.4 Solid state ^{13}C NMR

The solid-state ^{13}C NMR spectra for CR-TEL and AM-TEL were recorded using ECZR NMR spectrometer (JNM-ECA Series, JEOL Ltd., Tokyo, Japan) operated at 400 MHz. Approximately 500 mg of powdered samples (CR-TEL and AM-TEL) were packed (separately) very tightly into standard 5 mm (outer diameter) ZrO_2 rotors provided with a Kel-F cap and JEOL FG NMR tunable probe. All spectra were recorded at room temperature and processed with Delta software (version 4.3), and graph were generated using GraphPad Prism version 5.00 for Windows, GraphPad Software, San Diego California USA, www.graphpad.com.

3 Results and Discussion

3.1 Spectral differences in CR-TEL and AM-TEL.

Structurally, TEL (Fig. 1) has a biphenyl fragment with an acidic moiety (acid carboxylic group) that is attached to benzimidazole moiety through a methylene group [39]. TEL molecule has one

potential hydrogen bond donor (HBD) and six hydrogen bond acceptors (HBAs) (Supplementary information Table S1). Both, HBA and HBD groups are the potential sites for the association/interaction of molecules during the course of crystallization process in which molecules are arranged themselves into a three-dimensionally ordered phase. Several studies [23,24,40] have shown that generation of amorphous solids led to a reduction in the intensity of FTIR peaks. Thus, loss of spectral resolution is attributed to amorphization process. In this study, AM-TEL was prepared by quench cooling of the CR-TEL melt and confirmed using various tools like polarised light microscopy (PLM), differential scanning calorimetry (DSC) and powder X-ray diffraction (PXRD) analysis (Supporting information, Fig S2-S3). AM-TEL exhibited characteristic glass transition temperature at 133°C (heating rate 20°C/min) and showed a PXRD pattern devoid of distinct diffraction peaks at characteristic scattering 2θ angles. In CR-TEL (Fig. 3), polar hydrogen atom (H^{52}), covalently attached to oxygen atom (O^{51}), hydrogen bonds with nitrogen atom (N^{54}) of terminal benzimidazole fragment of neighbour TEL molecule present in the same antiparallel sheet [31]. Thus, it can be assumed that during quench cooling, molecular rearrangements occur and acid hydroxyl group may acquire different orientations leading to generation of AM-TEL. Hence, AM-TEL might have altered spectral properties of acid carbonyl and acid hydroxyl groups. The peaks (cf. Fig. 2A) positioned at 3027 cm^{-1} and 3059 cm^{-1} are associated with acid hydroxyl group of CR-TEL [32]. However, in AM-TEL, relative peak intensity of these peaks was greatly reduced and there was found a hump with peak maxima at 3007 cm^{-1}. This shift ($\Delta\upsilon$ = 20 cm^{-1}) to lower wavenumber (3027 cm^{-1} to 3007 cm^{-1}) might be associated to participation of acid hydroxyl group in some intermolecular interactions different from that were present in CR-TEL. The two broad peaks of similar intensity (Fig. 2B) positioned at 1933 cm^{-1} and 2466 cm^{-1} were observed in CR-TEL. These peaks are characteristic of -COOH group, hydrogen bonded to an aromatic ring nitrogen atom [41]. In AM-TEL, these peaks were broadened to great extent. This might be due to alterations in conformations during melt quench cooling and formation of AM-TEL.

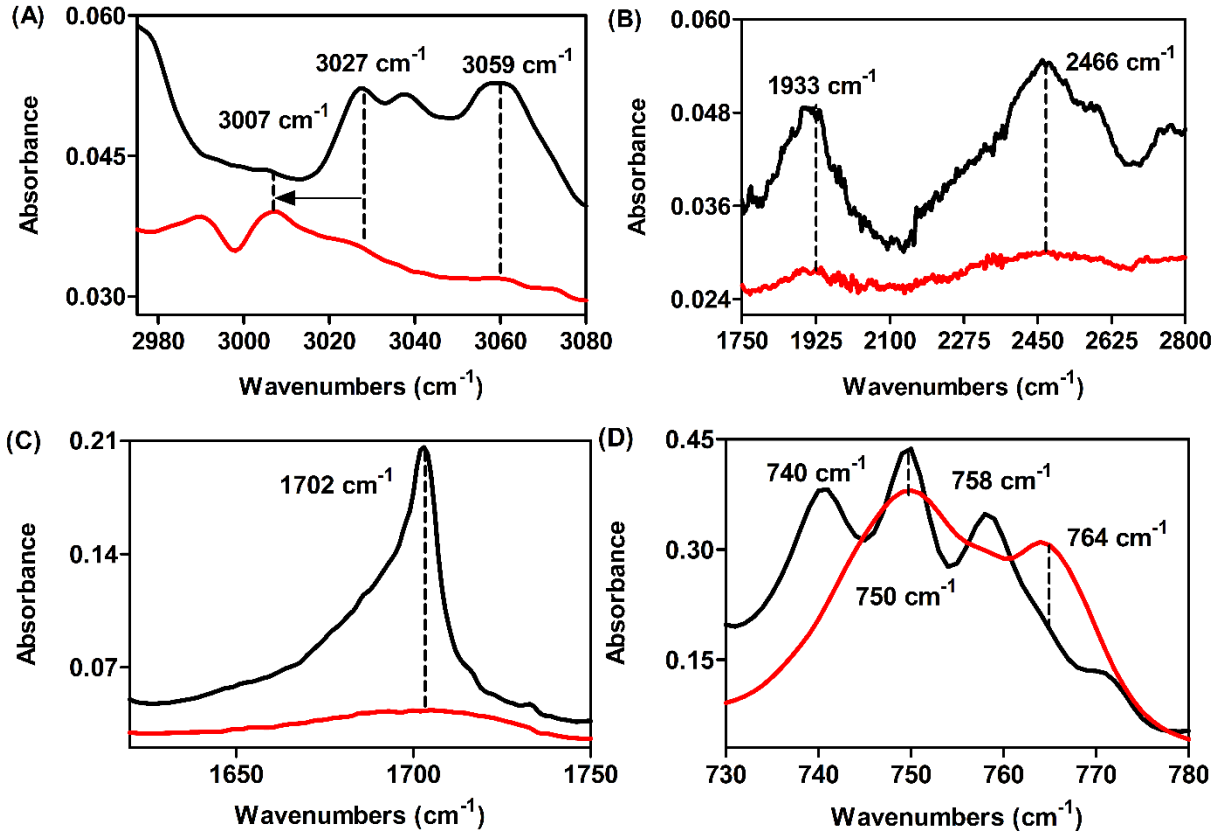

Fig. 2. Comparative display of partial ATR-FTIR spectra of CR-TEL (black) and AM-TEL (red): (A) Acid hydroxylic group stretching, (B) Aromatic ring nitrogen (Ar-N) stretching, (C) Acid C=O stretching and (D) C-H stretching of disubstituted benzene ring.

As depicted in the Fig. 2C, a strong and sharp peak attributed to non-hydrogen bonded acid carbonyl group is positioned at 1702 cm^{-1} [23,42]. On the contrary, in AM-TEL, this peak was observed at the same position. However, the peak becomes very broad with a reduced relative peak intensity. This broadening of the peak might be due to involvement of a carbonyl group in some interactions revealing a change in local environment. The peaks (cf. Fig. 2D) at 740 cm^{-1}, 750 cm^{-1} and 758 cm^{-1} in CR-TEL are associated to C-H wagging vibrations of disubstituted benzene ring [43]. However, in AM-TEL, only peaks at 750 cm^{-1} and 765 cm^{-1} were observed. This shift in wave number might be associated with an increased interaction of aromatic C-H with other functionalities of TEL molecule leading to higher conformational flexibility in AM-TEL.

3.2 Molecular interactions of CR-TEL

The analysis of single-crystal X-ray diffractometric data (cif file) of TEL [31] using the Mercury software facilitated the visualization of arrangement of TEL molecules in its unit cell (Fig. 3).

It was observed that the TEL unit cell contains 4 TEL molecules (i.e., Z = 4) arranged in two antiparallel sheets (sheet 1: green and yellow molecules; sheet 2: white and violet molecules) in which molecules of sheet-1 do not interact with molecules of sheet 2; however, molecules within a sheet interact with each other through inter-molecular hydrogen bonds (InterHBs). For instance, in antiparallel sheet 1, there is an InterHB (represented by dotted lines) between $-O^{51}-H^{52}$ (yellow) and N^{54} of adjacent TEL molecule (green). Thus, TEL molecules in its crystalline state form sheets of $O^{51}-H^{52}\ldots N^{54}$ hydrogen bonds ($H^{52}\ldots N^{54}$ 2.6 Å, H^{52}-N^{54} 1.68 Å and an angle of 166.19° between H^{52}-N^{54}). This represents abundant, most preferred and favourable hydrogen bonding pattern among disubstituted benzimidazole derivatives. The above observation is also in agreement with the Kitogorodoski principle of molecular crystal packing [44].

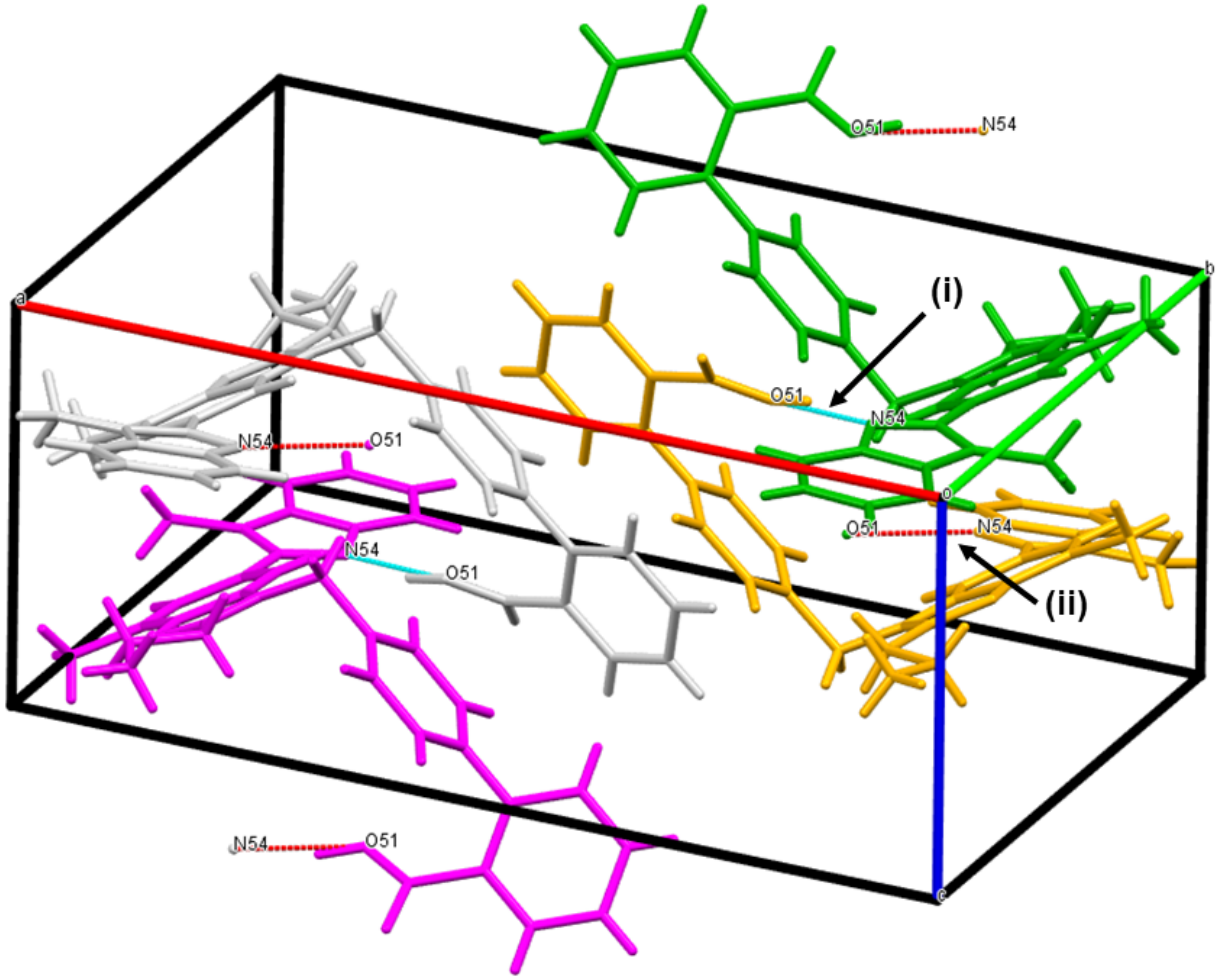

Fig. 3: Unit cell of TEL showing hydrogen-bonding pattern for CR-TEL. Hydrogen atom covalently bonded to O^{51} atom is hydrogen bonded (dotted lines) to N^{54} atom. The figure was drawn using the Mercury program (version 4.0.0) and the cif file.

3.3 Molecular dynamics simulations of CR-TEL and AM-TEL

Unrestrained molecular dynamic simulations clearly indicates that CR-TEL (Fig. 4A) forms a well-defined 3D long-range pattern of molecular arrangement as compared to AM-TEL (Fig. 4B). Furthermore, the pattern of hydrogen bonding in CR-TEL (Fig. 4C) and AM-TEL (Fig. 4D) was neither similar nor to same extent. The number of possible InterHBs interactions in CR-TEL were strong but very few (Supplementary information Table S2). On contrary, in AM-TEL, the number of possible molecular interactions (InterHBs and IntraHBs) are much higher when compared to CR-TEL.

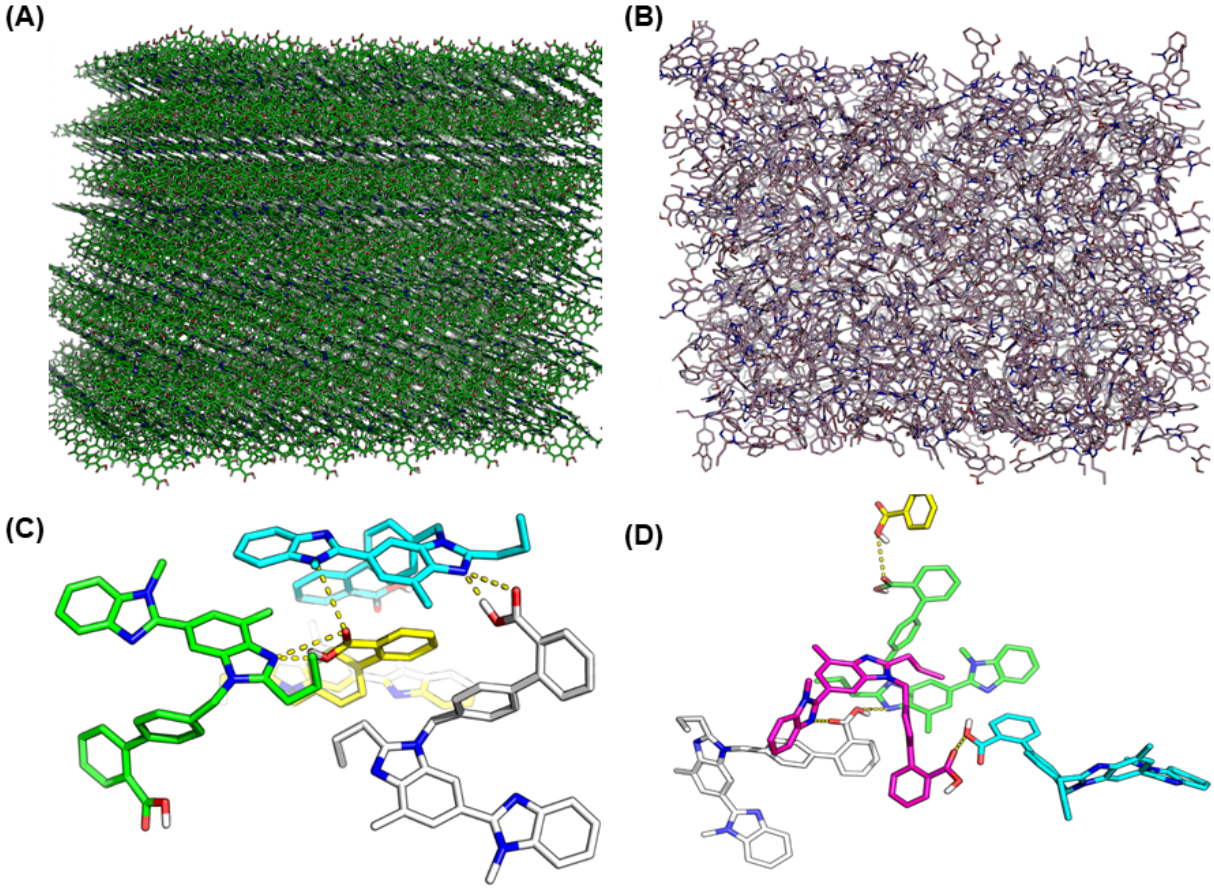

Fig. 4. Comparison of molecular arrangement of TEL from independent CR-TEL (A) and AM-TEL (B) molecular dynamics simulations snapshots. Various molecular interactions are highlighted from MD simulation snapshots for CR-TEL (C) and AM-TEL (D). Hydrogen bonds are indicated by yellow dotted lines.

Furthermore, an investigation of the molecular populations of CR-TEL and AM-TEL revealed that in CR-TEL more than 74% structures showed interHBs (620 average number of hydrogen bonds); however, in case of AM-TEL only 2.4% structures showed interHBs (9 average number of hydrogen bonds) (Fig. 5).

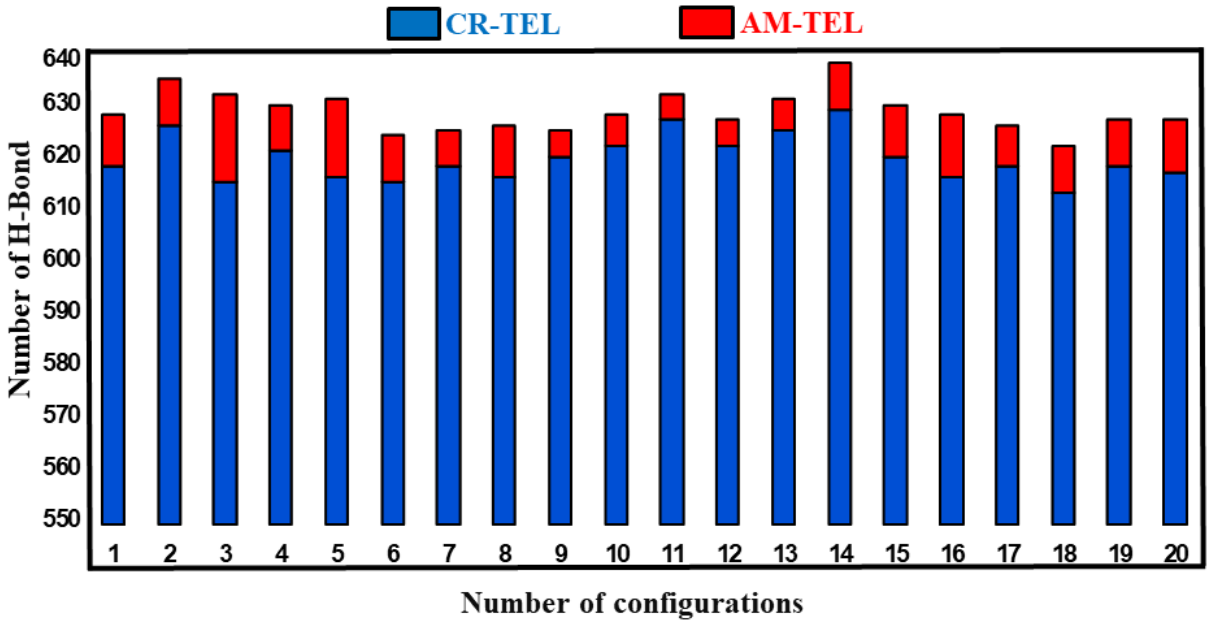

Fig. 5 Hydrogen bonds populations observed in CR-TEL and AM-TEL

A striking difference was observed in life time (Table 1) of the hydrogen bonds where more than 470 hydrogen bonds had 100% life time i.e., they are observed in all the snapshots and a total of 507 hydrogen bonds had a lifetime greater than 50%. In the case of AM-TEL, the largest observed life time for a hydrogen bond was 28% and only 7 of the hydrogen bonds (from a total of 330) had more than 1% life time. Another interesting observation was that in CR-TEL only interHBs were observed while in case of AM-TEL there was also non-zero population of intraHBs (N^{54}… $H^{52}O^{51}$). It was observed that the hydrogen bond lengths for N^{54} … H^{52} - O^{51} and O^{50} … H^{52} - O^{51} in CR-TEL were shorter than that of AM-TEL. This indicates that weaker hydrogen bonds in AM-TEL result from rearrangement of stronger hydrogen bonds of CR-TEL during the melt's quench cooling, might be responsible for formation of AM-TEL. This hypothesis can be explained on basis of differences in the participating atoms in the hydrogen bonding. In CR-TEL, H^{52} atom (covalently bonded to O^{51} atom) hydrogen bonds to N^{54} atom of terminal benzimidazole fragment of neighbour TEL molecule present in same antiparallel sheet. On contrary, in AM-TEL, strong HBD (-OH group) preferentially hydrogen bonds to stronger HBA (C=O). However, in presence of abundant weaker HBAs (N atoms associated to aromatic ring), this arrangement might not occur which may lead to the appearance of CR-TEL.

Table 1: Summary of molecular interactions obtained CR-TEL and AM-TEL from molecular dynamics trajectories (10 ns time scale).

Molecular interactions	CR-TEL		AM-TEL	
	Bond length (Å), Bond angle	Life time (%)	Bond length (Å), Bond angle	Life time (%)
N^{54}… $H^{52}O^{51}$ (inter)	2.73, 156.51	100	2.94, 158.53	4
O^{51}… $H^{52}O^{51}$ (inter)	-	-	2.90, 158.62	28
N^{54}… $H^{52}O^{51}$ (inter)	-	-	2.92, 151.48	12
O^{52}… $H^{52}O^{51}$ (inter)	-	-	2.93, 154.79	4
N^{54}… $H^{52}O^{51}$ (intra)	-	-	2.92, 145.93	7

In addition, radial distribution function (RDF) was also investigated for CR-TEL and AM-TEL (Supporting information, S4). The results revealed that CR-TEL showed well defined peaks which are generally observed for molecules in crystalline environments. However, these were absent in case of AM-TEL which is due to loss of translational degrees of freedom**.**

3.4 Solid state ^{13}C NMR

In addition to molecular dynamics simulations, ^{13}C solid-state NMR (Supporting information, Fig. S5-S6 and Table S2) was also used to investigate the molecular interactions in CR-TEL and AM-TEL as bulk level methods (cf. DSC and PXRD analysis) do not provide localised chemical information on crystalline and amorphous forms. An overlay of ^{13}C solid-state NMR spectra of CR-TEL and AM-TEL (Fig. 6) revealed that CR-TEL showed sharp resonances which are characteristics of ordered materials [45]. On the contrary, AM-TEL shows broad or diffused peaks of poor resolution which indicates highly disordered materials [46,47]. The resonances were assigned on the basis of solution state ^{13}C NMR [48] and ^{13}C spectral assignments given in Fig. 6 refer to numbering scheme shown for TEL in Fig. 1. Fig. 6A displayed resonances (10 to 50 ppm) assigned to the carbons of aliphatic chain (C^{26}, C^{27}, C^{28}), methyl group (C^{39} and C^{38}) and imidazole group (C^{16}). Fig. 6B and 6C showed resonances (105 to 145 ppm) assigned to the carbons of phenyl rings (C^{25}, C^{37}, C^{34}, C^{35}, C^{36}, and C^{12}, C^{11}, C^{7}, C^{21}, C^{10}, C^{24}, C^{32} and C^{3}). Fig. 6D showed resonances (150 to 175 ppm) attributed to carbons of imidazole (C^{18} and C^{30}) and acid carbonyl group (C^{1}). The major difference between CR-TEL and AM-TEL were observed for carbons (Fig. 6D) directly bonded to the carbonyl oxygen (C^{1}) and imidazole carbons (C^{30} and C^{18}). These findings were also supported by ATR-FTIR spectra (Fig. 2) where AM-TEL showed a significant difference in the peak intensity assigned to the carbonyl

group (group directly bonded to C^1). Furthermore, these carbons (C^1, C^{30}, C^{18}) are also associated with torsion angle changes during the simulated annealing process used to investigate the intermolecular hydrogen bonding patterns in CR-TEL [31]. Thus, carbons C^1, C^{30} and C^{18} might be associated with the change in the conformations of TEL molecule in AM-TEL.

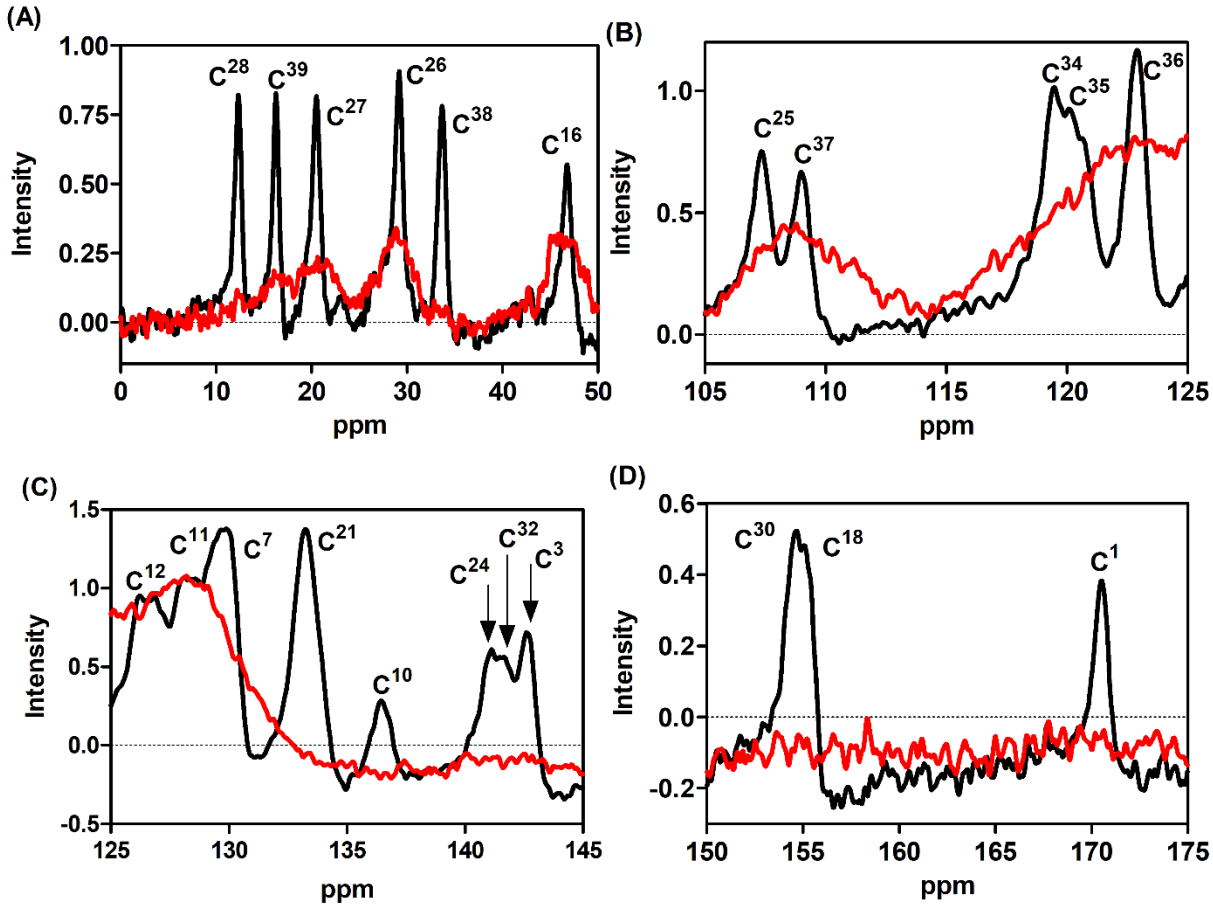

Fig. 6. Solid state ^{13}C NMR spectra of CR-TEL (black) and AM-TEL (red); aliphatic and imidazole carbons (A), phenyl ring carbons (B), phenyl. and imidazole ring carbons (C), imidazole and acid carbons (D).

4 Conclusions

Significant differences are observed in intermolecular interactions in CR-TEL and AM-TEL. A well-ordered network of intermolecular H-bonding was observed in CR-TEL for its potential hydrogen bond donor group (H^{52} covalently bonded to O^{51}) with the hydrogen bond acceptor group (N^{54} atom of central benzimidazole moiety). In contrast, AM-TEL exhibited a disordered molecular arrangement with relatively weaker intra- and intermolecular H-bonding between interacting groups. These reformed configurations of the molecular arrangements in AM-TEL

were supported by FTIR, ^{13}C solid state NMR studies. Furthermore, molecular dynamics simulation also confirmed these observations. From the observations of this study, we emphasize that molecules with an inclusive approach for interaction, due to presence of various hydrogen bond donor and acceptor groups, could stance a number of possibilities for transformed molecular conformations in different crystalline and amorphous forms. These differences in the 'microstructures' of the amorphous form could get translated into a characteristically different 'macro-state' as compared with their crystalline counterparts. Information about these differences in molecular associations could help in sensible picking of excipients that could explicitly interact with the molecules and thus can limit the molecular mobility of amorphous phase.

ACKNOWLEDGMENTS

This project is funded by grant from University Grant Commission (UGC), New Delhi (India) (UGC Letter No. F1-17.1/2014-15/RGNF-2014-15-SC-UTT-62448 /(SA-III/Website).

REFERENCES

(1) Gribbon, P.; Andreas, S. High-Throughput Drug Discovery: What Can We Expect from HTS? *Drug Discov. Today* **2005**, *10* (1), 17–22. https://doi.org/10.1016/S1359-6446(04)03275-1.

(2) Macalino, S. J. Y.; Gosu, V.; Hong, S.; Choi, S. Role of Computer-Aided Drug Design in Modern Drug Discovery. *Arch. Pharm. Res.* **2015**, *38* (9), 1686–1701. https://doi.org/10.1007/s12272-015-0640-5.

(3) Di, L.; Fish, P. V.; Mano, T. Bridging Solubility between Drug Discovery and Development. *Drug Discov. Today.* **2012**, *17* (9–10), 486–495. https://doi.org/10.1016/j.drudis.2011.11.007.

(4) Burton, P. S.; Goodwin, J. T.; Vidmar, T. J.; Amore, B. M. Predicting Drug Absorption: How Nature Made It a Difficult Problem. *J. Pharmacol. Exp. Ther.* **2002**, *303* (3), 889–895. https://doi.org/10.1124/jpet.102.035006.

(5) Aaltonen, J.; Alleso, M.; Mirza, S.; Koradia, V.; Gordon, K. C.; Rantanen, J. Solid Form Screening - A Review. *Eur J Pharm Biopharm* . **2009**, *71* (1), 23–37. https://doi.org/10.1016/j.ejpb.2008.07.014.

(6) Singhal, D.; Curatolo, W. Drug Polymorphism and Dosage Form Design: A Practical Perspective. *Adv. Drug Deliv. Rev.* **2004**, *56* (3), 335–347.

https://doi.org/10.1016/j.addr.2003.10.008.

(7) Aakeroy, C. B.; Fasulo, M. E.; Desper, J. Cocrystal or Salt: Does It Really Matter? *Mol. Pharm* **2007**, *4* (3), 317–322. https://doi.org/10.1021/mp060126o.

(8) Berge, S. M.; Bighley, L. D. . M. Pharmaceutical Salts. *J. Pharm. Sci.* **1977**, *66* (1), 1–19. https://doi.org/10.1002/jps.2600660104.

(9) Bolla, G.; Nangia, A. Pharmaceutical Cocrystals: Walking the Talk. *Chem. Commun* **2016**, *52* (54), 8342–8360. https://doi.org/10.1039/c6cc02943d.

(10) Yu, L. Amorphous Pharmaceutical Solids: Preparation, Characterization and Stabilization. *Adv. Drug Deliv. Rev.* **2001**, *48* (1), 27–42. https://doi.org/10.1016/S0169-409X(01)00098-9.

(11) Murdande, S. B.; Pikal, M. J.; Shanker, R. M.; Bogner, R. H. Solubility Advantage of Amorphous Pharmaceuticals: I. a Thermodynamic Analysis. *J. Pharm. Sci.* **2010**, *99* (3), 1254–1264. https://doi.org/10.1002/jps.21903.

(12) Gupta, P.; Chawla, G.; Bansal, A. K. Physical Stability and Solubility Advantage from Amorphous Celecoxib: The Role of Thermodynamic Quantities and Molecular Mobility. *Mol. Pharm.* **2004**, *1* (6), 406–413. https://doi.org/10.1021/mp049938f.

(13) Wojnarowska, Z.; Grzybowska, K.; Hawelek, L.; Dulski, M.; Wrzalik, R.; Gruszka, I.; Paluch, M.; Pienkowska, K.; Sawicki, W.; Bujak, P.; Paluch, K. J.; Tajber, L.; Markowski, J. Molecular Dynamics, Physical Stability and Solubility Advantage from Amorphous Indapamide Drug. *Mol. Pharm.* **2013**, *10* (10), 3612–3627. https://doi.org/10.1021/mp400116q.

(14) Babu, N. J.; Nangia, A. Solubility Advantage of Amorphous Drugs and Pharmaceutical Cocrystals. *Cryst. Growth Des.* **2011**, *11* (7), 2662–2679. https://doi.org/10.1021/cg200492w.

(15) Hilden, L. R.; Morris, K. R. Physics of Amorphous Solids. *J. Pharm. Sci.* **2004**, *93* (1), 3–12. https://doi.org/10.1002/jps.10489.

(16) Kaushal, A. M.; Gupta, P.; Bansal, A. K. Amorphous Drug Delivery Systems: Molecular Aspects, Design, and Performance. *Crit Rev Ther Drug Carr. Syst* **2004**, *21* (3), 133–193. https://doi.org/10.1615/CritRevTherDrugCarrierSyst.v21.i3.10.

(17) Hancock, B. C.; Zografi, G. Characteristics and Significance of the Amorphous State in Pharmaceutical Systems. *J. Pharm. Sci.* **1997**, *86* (1), 1. https://doi.org/10.1021/js9601896.

(18) Hancock, B. C. Disordered Drug Delivery: Destiny, Dynamics and the Deborah Number.

J. Pharm. Pharmacol. **2002**, *54* (6), 737–746. https://doi.org/10.1211/0022357021778989.

(19) Zhu, H.; Sacchetti, M. Solid State Characterization of an Neuromuscular Blocking Agent - GW280430A. *Int. J. Pharm.* **2002**, *234* (1–2), 19–23. https://doi.org/10.1016/S0378-5173(01)00928-0.

(20) Wyttenbach, N.; Kuentz, M. Glass-Forming Ability of Compounds in Marketed Amorphous Drug Products. *Eur J Pharm Biopharm* . **2017**, *112*, 204–208. https://doi.org/10.1016/j.ejpb.2016.11.031.

(21) Aso, Y.; Yoshioka, S.; Kojima, S. Molecular Mobility-Based Estimation of the Crystallization Rates of Amorphous Nifedipine and Phenobarbital in Poly(Vinylpyrrolidone) Solid Dispersions. *J. Pharm. Sci.* **2004**, *93* (2), 384–391. https://doi.org/10.1002/jps.10526.

(22) Descamps, M.; Willart, J. F. Perspectives on the Amorphisation/Milling Relationship in Pharmaceutical Materials. *Adv. Drug Deliv. Rev.* **2016**, *100*, 51–66. https://doi.org/10.1016/j.addr.2016.01.011.

(23) Taylor, L. S.; Zografi, G. Spectroscopic Characterization of Interactions between PVP and Indomethacin in Amorphous Molecular Dispersions. *Pharm. Res.* **1997**, *14* (12), 1691–1698. https://doi.org/10.1023/A:1012167410376.

(24) Kaushal, A. M.; Chakraborti, A. K.; Bansal, A. K. FTIR Studies on Differential Intermolecular Association in Crystalline and Amorphous States of Structurally Related Non-Steroidal Anti-Inflammatory Drugs. *Mol. Pharm.* **2008**, *5* (6), 937–945. https://doi.org/10.1021/mp800098d.

(25) Wienen, W.; Entzeroth, M.; Meel, J. C. a.; Stangier, J.; Busch, U.; Ebner, T.; Schmid, J.; Lehmann, H.; Matzek, K.; Kempthorne-Rawson, J.; Gladigau, V.; Hauel, N. H. A Review on Telmisartan: A Novel, Long-Acting Angiotensin II-Receptor Antagonist. *Cardiovasc. Drug Rev.* **2006**, *18* (2), 127–154. https://doi.org/10.1111/j.1527-3466.2000.tb00039.x.

(26) Yang, L.; Shao, Y.; Han, H. K. Improved PH-Dependent Drug Release and Oral Exposure of Telmisartan, a Poorly Soluble Drug through the Formation of Drug-Aminoclay Complex. *Int. J. Pharm.* **2014**, *471* (1–2), 258–263. https://doi.org/10.1016/j.ijpharm.2014.05.009.

(27) Ruiz Picazo, A.; Martinez-Martinez, M. T.; Colon-Useche, S.; Iriarte, R.; Sanchez-Dengra, B.; Gonzalez-Alvarez, M.; Garcia-Arieta, A.; Gonzalez-Alvarez, I.; Bermejo, M.; Colon-Useche, S.; Iriarte, R.; Sanchez-Dengra, B.; Gonzalez-Alvarez, M.; Garcia-

Arieta, A.; Gonzalez-Alvarez, I.; Bermejo, M. In Vitro Dissolution as a Tool for Formulation Selection: Telmisartan Two-Step IVIVC. *Mol. Pharm.* **2018**, *15* (6), 2307–2315. https://doi.org/10.1021/acs.molpharmaceut.8b00153.

(28) Park, J.; Cho, W.; Cha, K.-H.; Ahn, J.; Han, K.; Hwang, S.-J. Solubilization of the Poorly Water Soluble Drug, Telmisartan, Using Supercritical Anti-Solvent (SAS) Process. *Int. J. Pharm.* **2013**, *441* (1–2), 50–55. https://doi.org/10.1016/j.ijpharm.2012.12.020.

(29) Dahan, A.; Miller, J. M.; Amidon, G. L. Prediction of Solubility and Permeability Class Membership: Provisional BCS Classification of the World's Top Oral Drugs. *AAPS J.* **2009**, *11* (4), 740–746. https://doi.org/10.1208/s12248-009-9144-x.

(30) Laad, P.; Shete, G.; Modi, S. R.; Bansal, A. K. Differential Surface Properties of Commercial Crystalline Telmisartan Samples. *Eur J Pharm Sci* . **2013**, *49* (2), 109–116. https://doi.org/10.1016/j.ejps.2013.02.017.

(31) Dinnebier, R. E.; Sieger, P.; Nar, H.; Shankland, K.; David, W. I. F. Structural Characterization of Three Crystalline Modifications of Telmisartan by Single Crystal and High-Resolution X-Ray Powder Diffraction. *J. Pharm. Sci.* **2000**, *89* (11), 1465–1479. https://doi.org/10.1002/1520-6017(200011)89:11<1465::AID-JPS9>3.0.CO;2-C.

(32) Chadha, R.; Bhandari, S.; Haneef, J.; Khullar, S.; Mandal, S. Cocrystals of Telmisartan: Characterization, Structure Elucidation, in Vivo and Toxicity Studies. *CrystEngComm* **2014**, *16* (36), 8375–8389. https://doi.org/10.1039/c4ce00797b.

(33) Moura Ramos, J. J.; Diogo, H. P. Thermal Behavior and Molecular Mobility in the Glassy State of Three Anti-Hypertensive Pharmaceutical Ingredients. *RSC Adv.* **2017**, *7* (18), 10831–10840. https://doi.org/10.1039/c7ra00298j.

(34) Adrjanowicz, K.; Grzybowska, K.; Kaminski, K.; Hawelek, L.; Paluch, M.; Zakowiecki, D. Comprehensive Studies on Physical and Chemical Stability in Liquid and Glassy States of Telmisartan (TEL): Solubility Advantages given by Cryomilled and Quenched Material. *Philos. Mag* **2011**, *91* (13–15), 1926–1948. https://doi.org/10.1080/14786435.2010.534742.

(35) MacRae, C. F.; Sovago, I.; Cottrell, S. J.; Galek, P. T. A.; McCabe, P.; Pidcock, E.; Platings, M.; Shields, G. P.; Stevens, J. S.; Towler, M.; Wood, P. A. Mercury 4.0: From Visualization to Analysis, Design and Prediction. *J. Appl. Crystallogr.* **2020**, *53* (1), 226–235. https://doi.org/10.1107/S1600576719014092.

(36). D.A. Case, H.M. Aktulga, K. Belfon, I.Y. Ben-Shalom, S.R. Brozell, D.S. Cerutti, T.E. Cheatham, III, G.A. Cisneros, V.W.D. Cruzeiro, T.A. Darden, R.E. Duke, G. Giambasu,

M.K. Gilson, H. Gohlke, A.W. Goetz, R. Harris, S. Izadi, S.A. Izmailov, C. Jin, K. Kasavajhala, M.C. Kaymak, E. King, A. Kovalenko, T. Kurtzman, T.S. Lee, S. LeGrand, P. Li, C. Lin, J. Liu, T. Luchko, R. Luo, M. Machado, V. Man, M. Manathunga, K.M. Merz, Y. Miao, O. Mikhailovskii, G. Monard, H. Nguyen, K.A. O'Hearn, A. Onufriev, F. Pan, S. Pantano, R. Qi, A. Rahnamoun, D.R. Roe, A. Roitberg, C. Sagui, S. Schott-Verdugo, J. Shen, C.L. Simmerling, N.R. Skrynnikov, J. Smith, J. Swails, R.C. Walker, J. Wang, H. Wei, R.M. Wolf, X. Wu, Y. Xue, D.M. York, S. Zhao, and P.A. Kollman (2021), Amber **2021**, University of California, San Francisco.

(37). Gaussian 09, Revision A.02, M. J. Frisch, G. W. Trucks, H. B. Schlegel, G. E. Scuseria, M. A. Robb, J. R. Cheeseman, G. Scalmani, V. Barone, G. A. Petersson, H. Nakatsuji, X. Li, M. Caricato, A. Marenich, J. Bloino, B. G. Janesko, R. Gomperts, B. Mennucci, H. P. Hratchian, J. V. Ortiz, A. F. Izmaylov, J. L. Sonnenberg, D. Williams-Young, F. Ding, F. Lipparini, F. Egidi, J. Goings, B. Peng, A. Petrone, T. Henderson, D. Ranasinghe, V. G. Zakrzewski, J. Gao, N. Rega, G. Zheng, W. Liang, M. Hada, M. Ehara, K. Toyota, R. Fukuda, J. Hasegawa, M. Ishida, T. Nakajima, Y. Honda, O. Kitao, H. Nakai, T. Vreven, K. Throssell, J. A. Montgomery, Jr., J. E. Peralta, F. Ogliaro, M. Bearpark, J. J. Heyd, E. Brothers, K. N. Kudin, V. N. Staroverov, T. Keith, R. Kobayashi, J. Normand, K. Raghavachari, A. Rendell, J. C. Burant, S. S. Iyengar, J. Tomasi, M. Cossi, J. M. Millam, M. Klene, C. Adamo, R. Cammi, J. W. Ochterski, R. L. Martin, K. Morokuma, O. Farkas, J. B. Foresman, and D. J. Fox, Gaussian, Inc., Wallingford CT, **2016.**

(38) Roe, D. R.; Cheatham, T. E. PTRAJ and CPPTRAJ: Software for Processing and Analysis of Molecular Dynamics Trajectory Data. *J. Chem. Theory Comput.* **2013**, *9* (7), 3084–3095. https://doi.org/10.1021/ct400341p.

(39) Martin, A. D.; Siamaki, A. R.; Belecki, K.; Gupton, B. F. A Convergent Approach to the Total Synthesis of Telmisartan via a Suzuki Cross-Coupling Reaction between Two Functionalized Benzimidazoles. *J. Org. Chem.* **2015**, *80* (3), 1915–1919. https://doi.org/10.1021/jo5025333.

(40) Wojnarowska, Z.; Grzybowska, K.; Adrjanowicz, K.; Kaminski, K.; Paluch, M.; Hawelek, L.; Wrzalik, R.; Dulski, M.; Sawicki, W.; Mazgalski, J.; Tukalska, A.; Bieg, T. Study of the Amorphous Glibenclamide Drug: Analysis of the Molecular Dynamics of Quenched and Cryomilled Material. *Mol. Pharm.* **2010**, *7* (5), 1692–1707. https://doi.org/10.1021/mp100077c.

(41) Trivedi, D. R.; Ballabh, A.; Dastidar, P. Supramolecular Assemblies in Salts and Co-Crystals of Imidazoles with Dicarboxylic Acids. *CrystEngComm* **2003**, *5* (64), 538–567. https://doi.org/10.1039/b309216j.

(42) Kaur, M.; Bhatia, R. K.; Pissurlenkar, R. R. S.; Coutinho, E. C.; Jain, U. K.; Katare, O. P.; Chandra, R.; Madan, J. Telmisartan Complex Augments Solubility, Dissolution and Drug Delivery in Prostate Cancer Cells. *Carbohydr. Polym.* **2014**, *101*, 614–622. https://doi.org/10.1016/j.carbpol.2013.09.077.

(43) Sangwai, M.; Vavia, P. Amorphous Ternary Cyclodextrin Nanocomposites of Telmisartan for Oral Drug Delivery: Improved Solubility and Reduced Pharmacokinetic Variability. *Int. J. Pharm.* **2013**, *453* (2), 423–432. https://doi.org/10.1016/j.ijpharm.2012.08.034.

(44) Brock, C. P.; Dunitz, J. D. Towards a Grammar of Crystal Packing. *Chem. Mater.* **1994**, *6* (8), 1118–1127. https://doi.org/10.1021/cm00044a010.

(45) Li, M.; Xu, W.; Su, Y. Trends in Analytical Chemistry Solid-State NMR Spectroscopy in Pharmaceutical Sciences. *Trends Anal. Chem* **2021**, *135*, 116152. https://doi.org/10.1016/j.trac.2020.116152.

(46) Agrawal, S.; Ashokraj, Y.; Bharatam, P. V.; Pillai, O.; Panchagnula, R. Solid-State Characterization of Rifampicin Samples and Its Biopharmaceutic Relevance. *Eur. J. Pharm. Sci.* **2004**, *22* (2–3), 127–144. https://doi.org/10.1016/j.ejps.2004.02.011.

(47) Skotnicki, M.; Apperley, D. C.; Aguilar, J. A.; Milanowski, B.; Pyda, M.; Hodgkinson, P. Characterization of Two Distinct Amorphous Forms of Valsartan by Solid-State NMR. *Mol. Pharm* **2015**, *13* (1), 211–222. https://doi.org/10.1021/acs.molpharmaceut.5b00646.

(48) Bakheit, A. H. H.; Abd-Elgalil, A. A.; Mustafa, B.; Haque, A.; Wani, T. A. Telmisartan. In *Profiles of Drug Substances, Excipients and Related Methodology*; 2015; Vol. 40, pp 371–429. https://doi.org/10.1016/bs.podrm.2015.01.003.